ORIGINAL ARTICLE

Decoding the complex internal chemical structure of garnet porphyroblasts from the Zermatt area, Western Alps

Kurt Bucher[1] 🆔 | Tobias Björn Weisenberger[2] | Oliver Klemm[3] | Sebastian Weber[4]

[1]Mineralogy & Petrology, University of Freiburg, Freiburg, Germany

[2]Iceland GeoSurvey (ÍSOR), Reykjavík, Iceland

[3]Im Laimacker, Merzhausen, Germany

[4]Sächsisches Landesamt für Umwelt, Landwirtschaft und Geologie, Freiberg, Germany

Correspondence
Kurt Bucher, Mineralogy & Petrology, University of Freiburg, Freiburg, Germany.
Email: bucher@uni-freiburg.de

Handling Editor: Donna Whitney

Abstract

Garnet is a prototypical mineral in metamorphic rocks because it commonly preserves chemical and textural features that can be used for untangling its metamorphic development. Large garnet porphyroblasts may show extremely complex internal structures as a result of a polycyclic growth history, deformation, and modification of growth structures by intra- and intercrystalline diffusion. The complex internal structure of garnet porphyroblasts from garnet–phengite schists (GPS) of the Zermatt area (Western Alps) has been successfully decoded. The centimetre-sized garnet porphyroblasts are composed of granulite facies garnet fragments overgrown by a younger generation of grossular-rich eclogite facies garnet. The early granulite facies garnet (G-Grt) formed from low-P, high-T metamorphism during a pre-Alpine orogenic event. The late garnet (E-Grt) is typical of high-pressure, low-temperature (HPLT) metamorphism and can be related to Alpine subduction of the schists. Thus, the garnet of the GPS are polycyclic (polymetamorphic). G-Grt formation occurred at ~670 MPa and 780°C, E-Grt formed at ~1.7 GPa and 530°C. The G-Grt is relatively rich in Prp and poor in Grs, while E-Grt is rich in Grs and poor in Prp. The Alm content (mol.%) of G-Grt is 68 of E-Grt 55. After formation of E-Grt between and around fragmented G-Grt at 530°C, the GPS have been further subducted and reached a maximum temperature of 580°C before exhumation started. Garnet composition profiles indicate that the initially very sharp contacts between the granulite facies fragments of G-Grt and fracture seals of HPLT garnet (E-Grt) have been modified by cation diffusion. The profiles suggest that Ca did not exchange at the scale of 1 μm, whereas Fe and Mg did efficiently diffuse at the derived maximum temperature of 580°C for the GPS at the scale of 7–8 μm. The Grt–Grt diffusion profiles resulted from spending $c.$ 10 Ma at 530–580°C along the P–T–t path. The measured Grt composition profiles are consistent with diffusivities of log $D_{MgFe} = -25.8$ m^2/s from modelled diffusion profiles. Mg loss by diffusion from G-Grt is compensated by Fe gain by diffusion from E-Grt to maintain charge balance. This leads to a distinctive Fe concentration profile typical of uphill diffusion.

KEYWORDS

diffusion, eclogite facies, garnet, porphyroblast, uphill diffusion

1 | INTRODUCTION

Garnet is perhaps the archetypal mineral of metamorphic rocks. It occurs in ultramafic, mafic, granitoid, and carbonate rocks, and is most typical in metamorphic shales and marl-stones. Garnet is present in many textures and has been extensively used to decipher complex mineral growth–deformation relationships (e.g. Cutts et al., 2010; George & Gaidies, 2017; Kelly, Hoisch, Wells, Vervoort, & Beyene, 2015; Thigpen et al., 2013). Garnet commonly shows heterogeneous non-equilibrium compositions, most commonly with a continuous chemical core–rim zonation. The chemical zoning has been related to various growth and fractionation processes (e.g. Baxter, Caddick, & Dragovic, 2017; Hollister, 1966; Jedlicka, Faryad, & Hauzenberger-Jedlicka, 2015). Relatively simply zoned garnet that grew during one prograde metamorphic process has been modelled quantitatively (Gaidies, Pattison, & de Capitani, 2011; Gaidies, Petley-Ragan, Charkraboty, Dasgupta, & Jones, 2015). Garnet tends to overgrow companion minerals in the matrix, which are then preserved as inclusions in the garnet and reflect the matrix mineral assemblage at the time and conditions of the growth of the garnet (e.g. Lu, Zhang, Du, & Bucher, 2009).

The distribution of chemical components in garnet can be strongly irregular and asymmetrical. These composition patterns have been related to multiple growth and resorption episodes in the history of the garnet. Resorption of garnet is possible at all metamorphic grades and releases garnet components to the rock matrix where they are used for forming other minerals (e.g. Droop & Bucher-Nurminen, 1984). Garnet often preserve the detailed growth history of a metamorphic episode (e.g. Loomis, 1983).

Growth zoning of garnet is susceptible to later modification by internal diffusion (e.g. Florence & Spear, 1991; Woodworth, 1977; Yardley, 1977). The length scale of cation diffusion in garnet during an orogenic cycle at a high temperature suggests that garnet zoning profiles have been modified even in large garnet (Caddick, Konopasek, & Thompson, 2010). However, there are examples of garnet from granulite facies rocks that preserve internal chemical zonation at > 850°C in regional metamorphism (e.g. Chen, Sun, You, & Malpas, 1998).

Garnet may grow during more than one orogenic cycle in a particular rock. Garnet overgrowing old detrital garnet grains has been reported from Alpine high-*P* metasediments of the Western Alps (Manzotti & Ballèvre, 2013). Polymetamorphic garnet have been recognized from Samos, Greece, where Variscan amphibolite facies garnet cores have been overgrown by Ca-rich garnet rims during Alpine high-*P* metamorphism (Feenstra, Petrakakis, & Rhede, 2007) and, in the Moine Supergroup of Scotland, garnet preserves up to three distinct metamorphic events (Cutts et al., 2010).

This paper analyses and decodes the complex internal chemical structure of composite garnet porphyroblasts from garnet–phengite schist in the Western Alps. The analysis shows that composite garnet possess a great potential for preserving a protracted geological history even if they do not overgrow and enclose matrix minerals. The porphyroblasts are built of two different garnet that have grown during two very different types of metamorphism, the first generation under granulite facies and the second generation under eclogite facies conditions. The internal structure of the porphyroblasts has been complicated by brittle deformation between the growth episodes of the two garnet. Finally, the two garnet have been subjected to post-growth diffusional exchange along their contacts. The presented quantitative models for diffusional transport between the two garnet constrain diffusivities and time-scales of diffusional transport. The stranded diffusion profiles indicate uphill diffusion of Fe forced by the charge balance requirement.

2 | GEOLOGICAL BACKGROUND

The garnet porphyroblasts presented in this paper occur in garnet–phengite schists (GPS) of the Theodul Glacier Unit (TGU) (Weber & Bucher, 2015), a 2 km long and 100 m thick slab of eclogite facies continental basement rocks within the Zermatt–Saas meta-ophiolite unit (ZSU) of the Western Alps (Figure 1). GPS, eclogite, and biotite gneiss are the tectonically interleaved rock types of the TGU. Lenses and blocks of eclogite from some centimetres to many metres in size are common within the Grt-Ph schists (all abbreviations for mineral names after Whitney & Evans, 2010). The composition of the TGU eclogites is distinctly different from the eclogites of the ZSU (Weber & Bucher, 2015). From TGU eclogite assemblages, Weber and Bucher (2015) obtained 2.1 ± 0.1 GPa and $580 \pm 65°C$ for the *P*–*T* conditions at maximum depth in the subduction zone. Lu-Hf garnet whole-rock ages of 56.5 ± 2.7 and 58.2 ± 1.4 Ma for two TGU eclogite samples indicate that eclogite facies metamorphism occurred in the Palaeocene (Weber et al., 2015).

The ZSU enclosing the TGU slab represents a fully developed Mesozoic ophiolite that has been subjected to high-*P* and locally ultra-high–pressure metamorphism (Angiboust, Agard, Jolivet, & Beyssac, 2009; Bucher, Fazis, de Capitani, & Grapes, 2005; Bucher & Grapes, 2009; Groppo, Beltrando, & Compagnoni, 2009; Rebay, Spalla, & Zanoni, 2012) during Cretaceous to Eocene subduction under the overriding Apulian plate (Bowtell, Cliff, & Barnicoat, 1994; Lapen et al., 2003; Rubatto, Gebauer, & Fanning, 1998; Rubatto & Hermann, 2003).

3 | METHODS

The composition of the minerals was determined using a CAMECA SX-100 electron microprobe at the University of
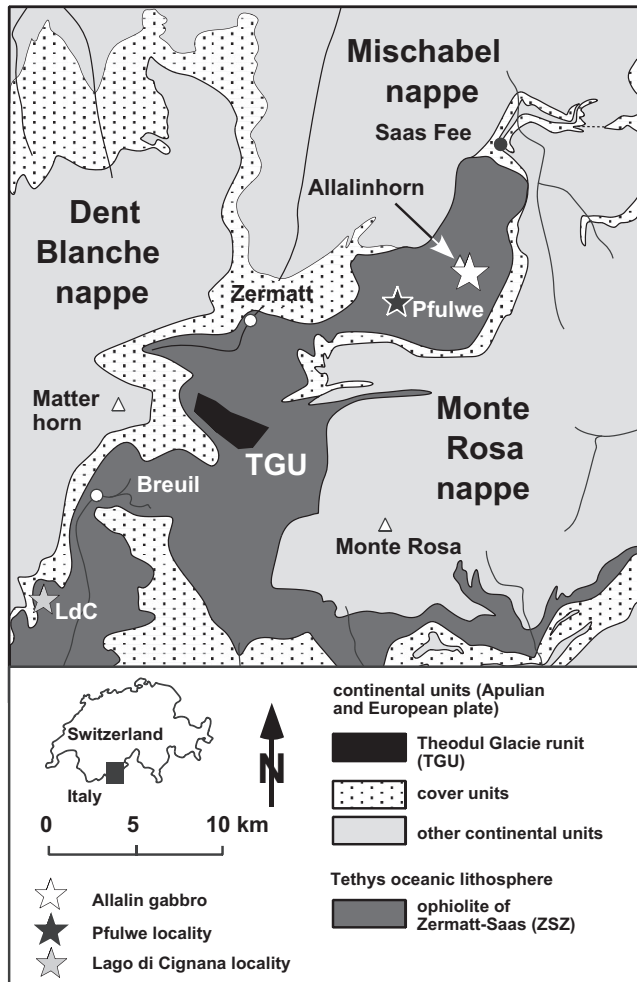
FIGURE 1 Simplified tectonic map of the Zermatt–Saas ophiolite zone (modified after Bearth, 1967). The Mischabel and Monte Rosa nappe are Penninic crystalline basement (European plate), the Dent Blanche nappe represents Austroalpine continental basement (Apulian plate). TGU = Theodul Glacier Unit (Weber & Bucher, 2015), LdC = Lago di Cignana coesite locality (Reinecke, 1991, 1998), eclogitic pillow lavas at Pfulwe locality (Bucher et al., 2005), eclogite facies metagabbro at Allalinhorn (Bucher & Grapes, 2009). The centre of the TGU outcrops is located at N 46°58′6.24″ and E 7°42′53.28″

Freiburg. All quantitative analyses were made using wavelength-dispersive spectrometers. Operating conditions were 15 kV acceleration voltage and 15–20 nA beam current with counting times of 10 s and a focussed electron beam. Mica was measured with a defocussed beam to minimize the effect of Na and K loss during analysis. The instrument was calibrated for each element analysed using well-characterized natural materials as standards. Data reduction was performed utilizing software provided by CAMECA.

Whole-rock analysis was performed by standard X-ray fluorescence techniques at the University of Freiburg, Germany, using a Philips PW 2404 spectrometer. Pressed powder and Li-borate–fused glass discs were prepared to measure contents of trace and major elements, respectively.

Raw data were processed with the standard XR-55 software from Philips. Relative standard deviations are <1 and <4% for major and trace elements, respectively. Loss on ignition was determined by heating at 1,100°C for 2 hr.

The $P–T$ conditions during garnet growth have been deduced from assemblage stability diagrams and assemblage models at $P–T$ using the Theriak/Domino software of de Capitani and Petrakakis (2010), and thermodynamic data from Berman (1988). The thermodynamics of garnet solutions and white mica follows the models of Berman (1988), and Keller, Capitani, and Abart (2005), respectively. Ideal site mixing has been used as a solution model for the phases: chlorite, biotite, epidote, and amphibole. The models consider the composition space $K_2O–Na_2O–CaO–FeO–MgO–Al_2O_3–SiO_2–H_2O–CO_2$ (KNCFMAS-HC). Thus, the models ignore Ti, Mn and P. Ti is present mainly in rutile and a very small modal amount of late titanite, while Mn is concentrated mainly in very thin rims around the fragments of garnet cores. Incorporating the small amount of Mn present in the main volume of garnet in the model slightly enlarges the stability domain of garnet but does not significantly modify derived $P–T$ conditions (Konrad-Schmolke, Zack, O'Brian, & Jacob, 2008). The oxidation state during G-Grt growth was fixed by the presence of graphite, which occurs as inclusions in G-Grt.

4 | RESULTS

4.1 | Petrography of the garnet–phengite schists

Samples of TGU garnet–phengite schist have been collected over the entire TGU exposure area during fieldwork from 2005 to 2015; however, most of the analysed and studied samples come from the hilltop (Point 3,030 m in elevation) ~500 m SW of the Trockener Steg cable car station. Two porphyroblastic garnet samples, KB860 and OK-Z133, yield particularly well-developed internal chemical structures and thus those samples are studied here in detail.

Most samples contain euhedral (locally elongated) garnet porphyroblasts and small euhedral garnet grains occurring in a matrix of phengite, plagioclase, chlorite, paragonite, and modally subordinate epidote, quartz, titanite, rutile, rare amphibole, and Fe sulphide. The Ph- and Chl-rich rocks are well foliated (Ph, Pg, Chl >70% modal). Some samples contain centimetre-sized euhedral garnet. The texture of some samples bears evidence for two generations of Ph. Garnet shows a bimodal size distribution. Large anhedral grains ranging from 0.1 to >2 cm in size are associated with Chl, Pl, Ph and Pg (Figure 2). Small subhedral to perfectly euhedral crystals occur in a uniform size range of 50–100 μm associated with quartz (Figure 2). These small Grt-Qz aggregates (lenses) are embedded in a matrix of Chl and white mica.
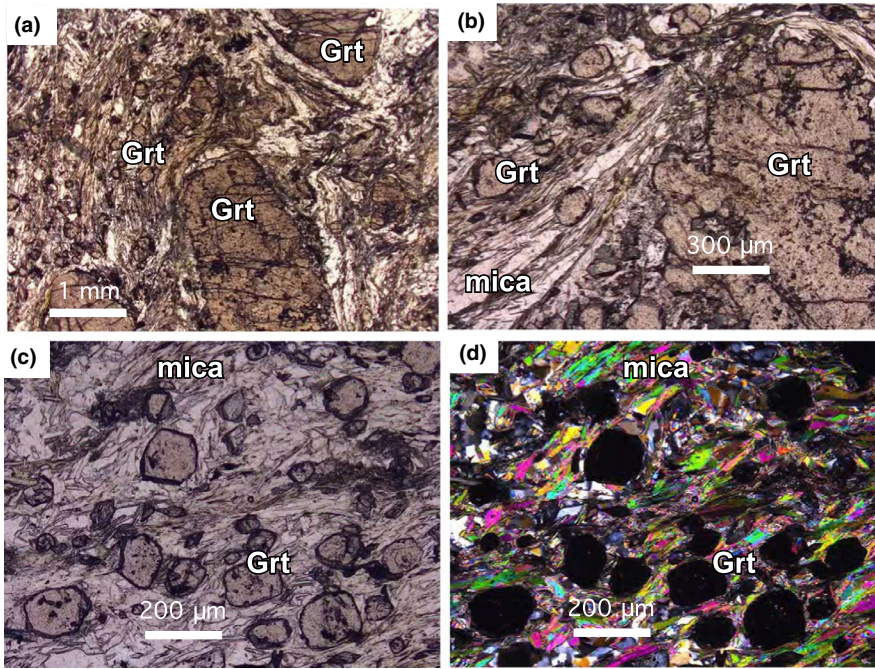
FIGURE 2 Photomicrographs of textures and mineral assemblages in sample KB860: (a) large garnet porphyroblast (plane polarized light); (b) rim of large garnet crystals in (plane polarized light); (c) small euhedral garnet in a matrix of quartz, plagioclase, white mica, and chlorite (plane polarized light); (d) same view under cross-polarized light
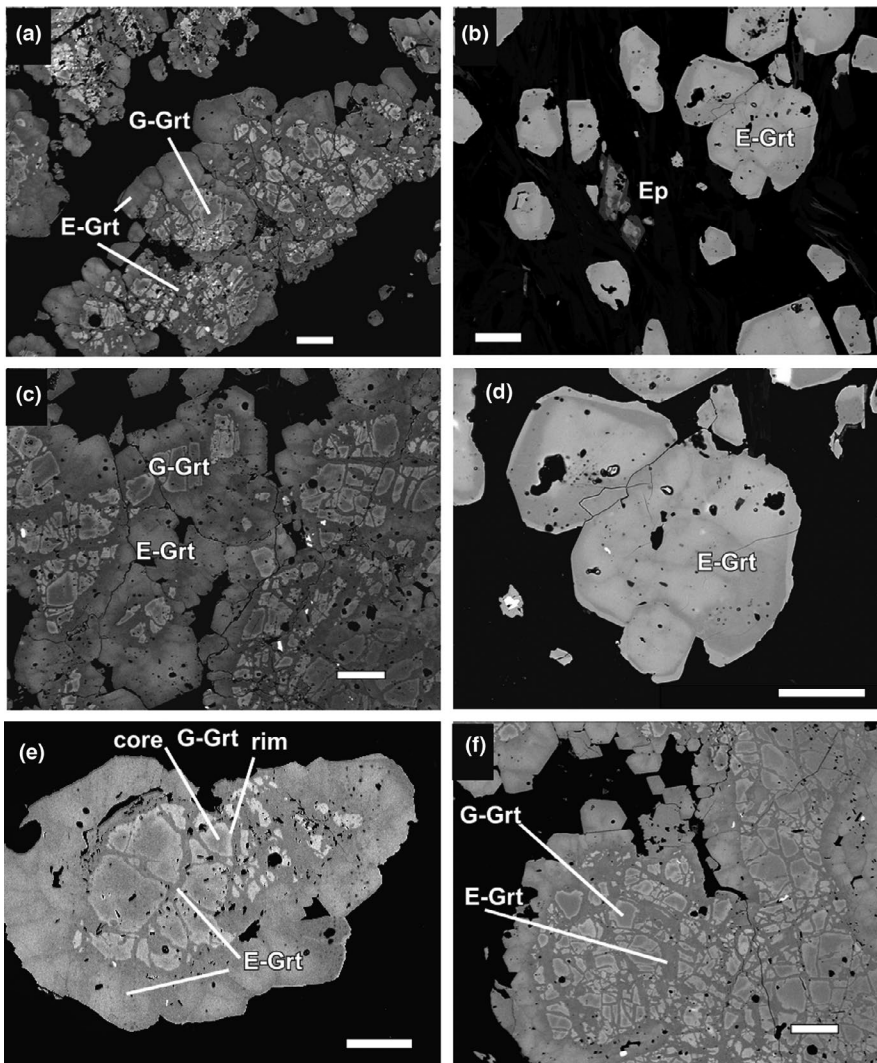

FIGURE 3 Backscattered electrons (BSE) overview images showing characteristic garnet porphyroblast textures in sample KB860. Scale bar = 100 μm. For detailed structures, see Figure 4 (a) Large garnet aggregate formed during two distinct garnet growth episodes. Fracture network generating fragments of G-Grt is undeformed. E-Grt forms euhedral subcrystals along the rims of porphyroblasts and seals the fracture network. (b) Subhedral to euhedral small grains of E-garnet. (c) Large fractured garnet porphyroblast showing internal zoning of fragments. (d) Smaller grains of coalesced E-Grt. (e) Smaller Grt porphyroblast showing the same fragmented internal structure as large porphyroblasts. (f) Large fragmented garnet with G-Grt fragments and E-Grt veins and overgrowth

Two generations of garnet can be recognized using back-scattered electron (BSE) images (Figures 3 and 4). Large porphyroblastic garnet crystals consist of an aggregate of angular and blocky fragments of first-generation garnet with a second generation of garnet material between the fragments and along the rims of the porphyroblasts (Figures 3 and 4). The BSE images indicate that the two distinct generations can also be distinguished based on their chemical composition (see below). Here, first-generation garnet will be denoted as G-Grt and second-generation garnet will be denoted as E-Grt.
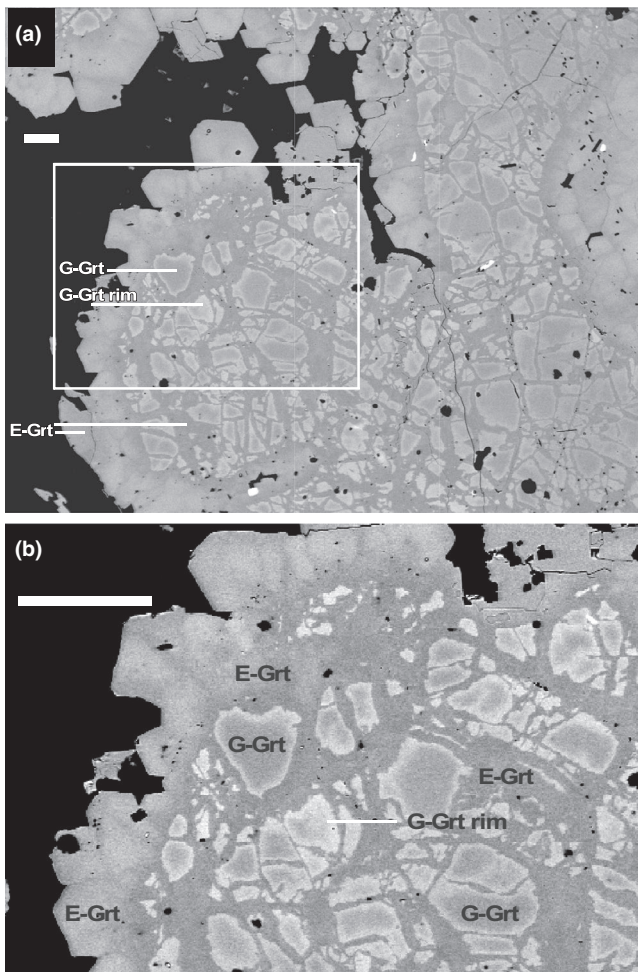

FIGURE 4 Backscattered electrons (BSE) images showing detailed internal chemical structure of a garnet porphyroblast in sample KB860. Scale bar = 100 μm. (a) Large garnet aggregate formed during two distinct garnet growth periods. Fracture network generating fragments of G-Grt is undeformed. E-Grt forms euhedral subcrystals along the aggregate rim and it seals the fracture network. Euhedral young garnet are particularly well developed in the upper left area of the figure. (b) Enlargement of the framed region of Figure 3. Fragments of early G-Grt are chemically zoned. G-Grt forms the dark core of the fragments, while brighter G-Grt rims of the fragments represent chemically modified parts of the original G-Grt fragments. Euhedral E-Grt at the rim shows faint veining

The chemically zoned G-Grt fragments occur as anhedral subgrains of 10–100 μm in size within large garnet crystals (Figures 3 and 4). The texture indicates that fragmentation of early G-Grt was followed by fracture sealing and overgrowth of the fragments by a younger generation of E-Grt. The G-Grt fragments themselves show a darker core area in BSE images, while very thin bright rims around the irregular shaped fragments are conspicuous on the BSE images. Garnet fragments in the core of large garnet aggregates show only a thin bright rim in contrast to fragments near the rims of large garnet showing relatively thick bright rims.

Late garnet occurs between fragments of G-Grt and forms euhedral subgrains along the porphyroblast rims (Figures 3 and 4). The fractures that cut the original G-Grt are straight and cross each other at high angles (Figures 3 and 4). Smaller euhedral E-Grt grains occur with only a few fragments of G-Grt. E-Grt also forms small perfectly euhedral grains often arranged in clusters in the matrix. They exhibit very weak concentric growth zonation and may show indistinct veining or sector growth patterns (Figures 3 and 4).

Early granulite facies garnet shows very rare and very small mineral inclusions of graphite, ilmenite, and Fe sulphide. No silicate mineral inclusions were found, except in sample OK-Z131 where garnet overgrows Chl. Mineral inclusions in E-Grt are virtually absent, except for a very few tiny grains of graphite and sulphide.

The dominant mica in the TGU is a fine-grained phengite. It is typically intergrown with Pg and also occurs as fine inclusions within Pg. Abundant Chl occurs in association with Ph and Pg and as a rare local replacement of Grt. In the foliated mica matrix of the rock, Chl locally grows across the foliation. Epidote occurs as small (<50 μm) euhedral grains with trapezoidal cross-section locally overgrowing corroded REE epidote (allanite). Plagioclase is a member of the matrix assemblage together with the white mica and chlorite. Amphibole occurs locally as a minor phase associated with chlorite. The presence of Chl-Ab pseudomorphs after amphibole rimmed by actinolite suggests that glaucophane was present in the rock at some earlier stage. Accessory titanite locally replaces rutile.

4.2 | Rock composition

The stable phase assemblage models using G-minimization techniques presented below require the chemical composition of the rock as input. The composition of the Grt-Ph schist sample KB860 is given in Table 1 together with the average composition of pelagic clay for comparison (Carmichael, 1989). KB860 differs by higher Al_2O_3, Fe_2O_3, and CaO, and lower SiO_2. KB860 is a terrigenous clastic rock and classifies as shale (Herron, 1988). The relatively high CaO of KB860 suggests that the shale contained carbonate (calcite) prior to the first metamorphism and that the sedimentary protolith classifies as calcareous mudstone.

TABLE 1 Composition of Grt-Ph schist KB860 and average pelagic shale

	KB 860	KB 860 anhydrous	Pelagic clay anhydrous
wt%			
SiO_2	49.34	50.75	60.80
TiO_2	1.16	1.19	0.86
Al_2O_3	22.80	23.45	18.38
Fe_2O_3	11.78	12.12	10.96
MnO	0.18	0.19	
MgO	3.19	3.28	3.77
CaO	3.82	3.93	0.80
Na_2O	1.68	1.73	1.44
K_2O	2.97	3.05	2.99
P_2O_5	0.12	0.12	
LOI	2.54		
Total	99.76	100	100

[a]Carmichael (1989), all Fe as Fe^{3+}.

4.3 | Chemical composition of minerals

4.3.1 | Garnet

The compositional structure of garnet in KB860 and OK-Z133 is shown in Figure 5. The element maps show that the G-Grt fragments generally are rich in almandine and pyrope component and E-Grt is rich in grossular component (Figure 6). Selected garnet analyses from the two samples are listed in Table 2a and b. Garnet has been analysed in sample KB860 in detail along two profiles across the fragmented inner part of the porphyroblasts (Figures 7 and 8). The full set of all 100 garnet analyses from two profiles of KB860 is given in Tables S1 and S2.

The garnet fragments (G-Grt) are generally pyrope-rich almandine garnet. The highest pyrope content of typically 28 mol.% Prp is found in the centre of the fragments of KB860. The fragments are concentrically chemically zoned. Pyrope decreases gradually from core to rim of the fragment, counterbalanced with a gradual increase in almandine towards the rims. Almandine increases sharply at the extreme edge of the fragments. Grossular and spessartine are constant inside the fragment. There is a remarkably high manganese concentration along the contact of G-Grt and E-Grt, where spessartine reaches a maximum of 8 mol.% in OK-Z133, and 6.5 mol.% in KB860. Background Sps in the fragments is 1.5 mol.% (Table 2a and b). Furthermore, grossular concentration is 5.5 mol.% with a range of ±0.1 in profile 1 fragments and 6 mol.% with a range of ±0.1 mol.% in the profile 2 fragment. The Grs content is constant to the very edge of the fragments (Figures 7 and 8).

Late garnet between the pyrope-rich fragments is rich in grossular containing up to 35.8 mol.% Grs component. Pyrope

is with ~8.5 mol.% Prp distinctly lower than in G-Grt (28%). E-Grt is quite constant in composition and shows no systematic zoning. The very small compositional variations are irregularly distributed (see also the BSE images inFigures 3 and 4).

The contact between G-Grt and E-Grt is very sharp and defined by the grossular content. It jumps from 6 to 35 mol.% over a distance of only 2–3 μm (Figures 7 and 8). The intermediate values occur at a 1–2 μm distance from the edge of E-Grt, which is at a distance of less than the resolution of the microprobe. This means that Grs is extremely discontinuous along the profiles in sharp contrast to the gradually changing Prp content varying between the typical G- and E-Grt values over distances of up to 10 μm. The Mn-rich zone visible on BSE images (Figures 3 and 4) as a bright rim around the fragments is located along the contact of the G-Grt fragments and E-Grt in the veins (Figures 7 and 8). The compositional structure of garnet porphyroblasts in the Grt-Ph schists is particularly well visible if the sum of Alm and Prp component is displayed together with Grs (Figure 9). This representation of the Grt composition shows that both G-Grt and E-Grt have a constant composition except for a very narrow zone at the Grt–Grt contact.

### 4.3.2 | Other silicate minerals

The composition of other silicate minerals occurring together with garnet in KB860 is given in Table 3. The abundant Ph marking the foliation has a rather uniform composition in all samples. The exception is pure Ms occurring as inclusion in Pg and late Ms growing across the foliation. Pg of constant composition contains a small amount of Ms component. All Chl is clinochlore. Ep shows strong chemical zoning. On BSE images a visible bright core indicates the presence of corroded allanite, the REE-rich variety of epidote. Some cores consist of Fe-free REE zoisite. The darker euhedral rims (BSE images) are composed of epidote (clinozoisite). The two types of amphibole present can be classified as barrosite and actinolite (Hawthorne et al., 2012), with Na of 0.75 and 0.16 apfu, respectively. At the rim of Chl+Ab pseudomorphs after Gln, actinolite overgrown by barroisite is locally present. Most plagioclase occurring in the matrix of the samples KB860, OK-Z131, and OK-Z133 is oligoclase of anorthite content An13–An18. In all samples, some albite is present, particularly in pseudomorphs after glaucophane.

4.4 | Modelled P–T conditions

4.4.1 | Conditions during growth of G-Grt

The presence of two generations of garnet with sharply contrasting composition suggests that the Grt-Ph schists possibly have experienced polycyclic metamorphism. The fragmented garnet

FIGURE 5 X-ray element maps showing the characteristic fragmented texture of large garnet cores (G-Grt), healed by a younger garnet generation (E-Grt). (a) Grain from sample KB860. G-Grt is low in Ca (blue colour), rich in Mg (green) and Fe (orange). E-Grt is rich in Ca (green), low in Mg (blue) and Fe (green). (b) Grain from sample OK-Z133 (Klemm, 2005). G-Grt is low in Ca (black), rich in Mg (yellow, orange) and Fe (orange). E-Grt is rich in Ca (yellow, orange), low in Mg (blue) and Fe (green). Very narrow thin spessartine-rich rims around G-Grt fragments are conspicuous
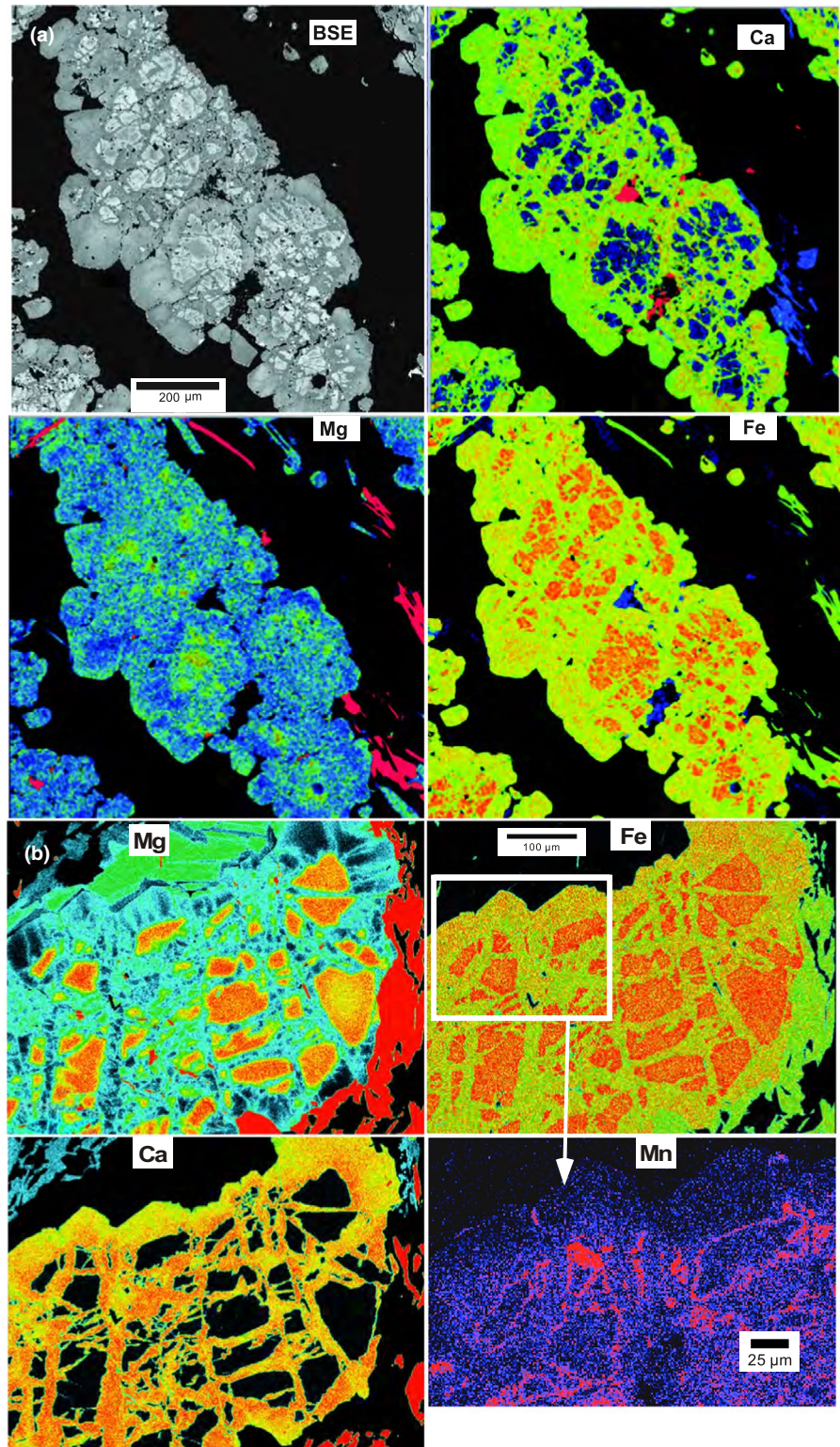
preserved in the inner areas of the large porphyroblasts is G-Grt. The composition of the central parts of the garnet fragments containing up to 28 mol.% pyrope and ~5 mol.% grossular (Table 2a and b) are typical of garnet from granulite facies metapelites (e.g. Markl, Bäuerle, & Grujic, 2000; Masberg, 2000).

The *P–T* conditions recorded by G-Grt of the GPS can be obtained from computed assemblage stability and garnet composition isopleth diagrams using the analysed bulk composition of the rock KB860 (Table 1). The diagram (Figure 10) models *P–T* during growth of G-Grt for the fluid composition given by the presence of excess graphite. Specifically, G-Grt of the composition Prp 28.5–Grs 5.5–Alm 66 has been used as a representative composition for G-Grt. This corresponds to G-Grt with the maximum measured Prp content.
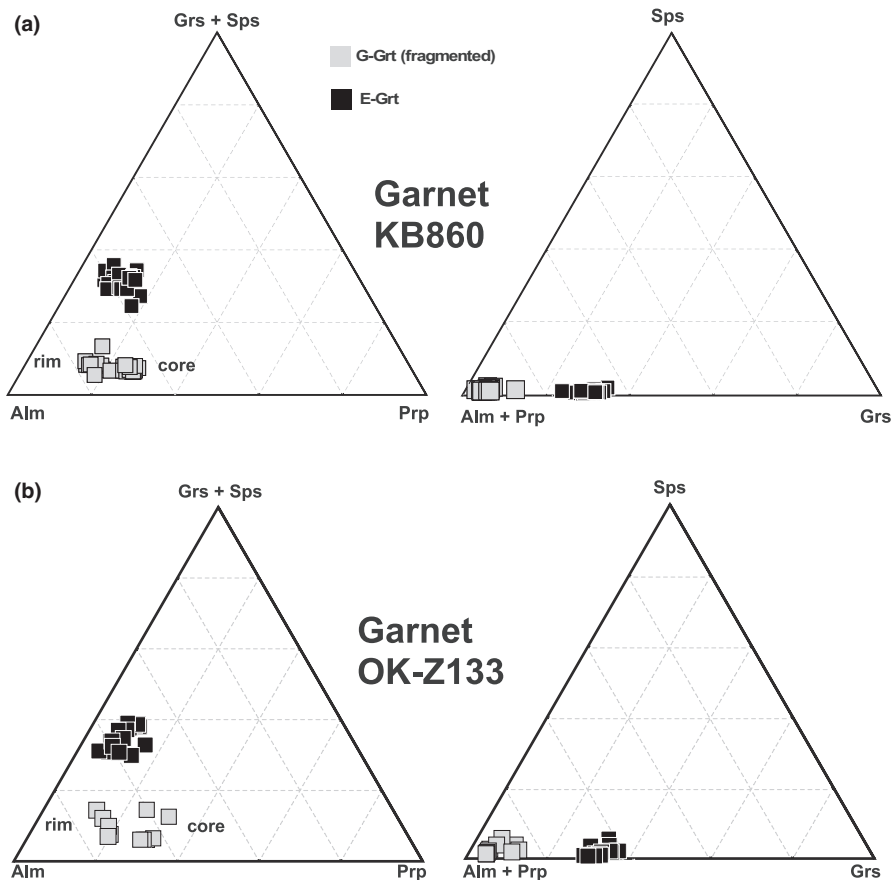
FIGURE 6 Compositional variation of garnet in sample KB860 and OK-Z133. Red squares = G-Grt, green squares = E-Grt. The porphyroblasts consist of two unconnected populations of Grt

The maximum Prp used in the model is justified by the likely presence of unzoned Prp-rich Grt at granulite facies conditions. Later processes all reduced Prp in Grt. For instance, cation diffusion between G-Grt and later E-Grt reduced Prp in the rims of G-Grt (see below).

The model predicts that G-Grt (Table 2a and b) formed at granulite facies conditions near 780°C ± 30 and 670 MPa ± 50 (Figure 10). At these conditions computed Grt composition (Prp 28, Grs 6, Alm 66) is identical to measured G-Grt. The predicted assemblage at 780°C and 670 MPa is (vol.%): Grt 26, Kfs 23, Pl 34, Bt 2, Crd 9, Sil 2, Qz 5, +Gr. From this assemblage garnet is the only mineral that survived later hydration and recrystallization. None of these assemblage minerals are present as inclusions in G-Grt porphyroblasts except fine dispersed graphite. At ~700 MPa, cordierite is not part of the predicted assemblage (Grt 27, Kfs 20, Pl 35, Bt 4, Sil 6, Qz 8). It has been replaced by Grt+Sil+Qz (Figure 10). Granulite facies metamorphism occurred most likely under low a_{H_2O} conditions indicated by the presence of graphite inclusions in G-Grt. Under low a_{H_2O} conditions, melting was not possible particularly because the maximum temperature was not excessively high (<800°C). Thus, the model assumes that the analysed bulk rock composition represents the rock during granulite facies metamorphism. Furthermore, it is also anticipated that garnet in the TGU schists is not of detrital origin in the original calcareous shale, like in some other HP

metasediments from the Alps (Manzotti & Ballèvre, 2013). The large G-Grt porphyroblasts in the TGU occur evenly distributed in an originally fine-grained clay-rich matrix (plus calcite), which is an unlikely depositional setting for centimetre-size detrital Grt grains.

4.4.2 | Conditions during growth of E-Grt

Grossular-rich garnet (E-Grt) formed both as fracture filling in and as an overgrowth on G-Grt porphyroblasts. It also occurs as euhedral small garnet in the matrix (Figures 3 and 4). The *P–T* conditions during the growth of E-Grt have been modelled using a reactive bulk composition derived from the total rock composition reduced by the computed amount of 26 vol.% G-Grt present at the granulite stage. This is the predicted equilibrium amount of G-Grt. The internal structure of the garnet porphyroblasts does not suggest massive resorption or dissolution of G-Grt during the post-granulite facies evolution. The maximum pyrope G-Grt has been used in deriving the reactive rock composition during E-Grt growth, in order to account for the later intra-garnet diffusion between G-Grt and E-Grt (see below). It is assumed that Grs-poor G-Grt was homogeneous and unzoned at temperatures close to 800°C. The model for the assemblage and the garnet composition uses H_2O excess conditions. Because E-Grt formed with increasing *T* and *P* during Alpine metamorphism of a

TABLE 2 (a) Selected typical analyses of G-Grt and E-Grt from three samples of TGU Grt-Ph schist (tables with single point analyses are provided as Supporting information), concentrations in wt%, cations per 12 oxygen, Grt endmember in mol.% (b) Garnet composition (selected analyses), concentrations in wt%, cations per 12 oxygen, mol. %

(a)

Sample/Point	KB860 p 1	KB860/p 1	KB860/p 2	KB860/p 2	KB860 p 1	KB860 p 1	KB860/p 2	KB860/p 2	OKZ129/1	OKZ129/2
	G-Grt	G-Grt	G-Grt	G-Grt	E-Grt	E-Grt	E-Grt	E-Grt	G-Grt	G-Grt
SiO_2	37.84	37.98	38.74	38.52	37.63	37.66	38.20	38.16	38.48	38.10
Al_2O_3	21.86	21.62	22.10	21.92	21.28	21.20	21.64	21.50	21.59	21.76
FeO	30.81	31.12	30.89	30.44	25.90	26.57	25.17	25.39	31.15	31.27
MnO	0.74	0.72	0.58	0.58	1.05	1.02	0.86	0.79	1.05	0.99
MgO	7.45	7.38	6.87	7.03	1.76	1.75	2.17	2.24	6.40	6.12
CaO	2.00	1.98	2.21	2.14	12.61	12.71	12.88	12.95	2.00	2.21
Total	100.69	100.79	101.39	100.63	100.23	100.91	100.92	101.03	100.67	100.45
Si	2.959	2.971	2.990	2.992	2.988	2.980	2.987	2.984	3.003	2.985
Al	2.015	1.993	2.010	2.006	1.991	1.977	1.994	1.982	1.985	2.009
Fe	1.973	1.994	1.994	1.977	1.684	1.722	1.645	1.661	2.033	2.049
Mn	0.049	0.047	0.038	0.038	0.071	0.068	0.057	0.052	0.069	0.066
Mg	0.868	0.861	0.790	0.814	0.209	0.207	0.253	0.261	0.745	0.715
Ca	0.168	0.166	0.183	0.178	1.073	1.078	1.079	1.085	0.167	0.186
Almandine	64.5	65.0	66.4	65.7	55.5	56.0	54.2	54.3	67.4	68.0
Spessartine	1.6	1.5	1.3	1.3	2.3	2.2	1.9	1.7	2.3	2.2
Pyrope	28.4	28.1	26.3	27.1	6.9	6.7	8.3	8.5	24.7	23.7
Grossular	5.5	5.4	6.1	5.9	35.3	35.0	35.6	35.5	5.5	6.2
X_{Fe}	0.69	0.70	0.72	0.71	0.89	0.89	0.87	0.86	0.73	0.74

TABLE 2 (Continued)

(b)

Sample/Point	OK-Z129/2 E-Grt	OK-Z131/1 E-Grt	OK-Z131/3 E-Grt	OK-Z133/11 G-Grt	OK-Z133/13 G-Grt	OK-Z133/17 E-Grt	OK-Z133/18 E-Grt	OK-Z133/19 E-Grt	OK-Z133/7 E-Grt	OK-Z133/10 E-Grt
SiO_2	38.59	38.38	38.46	38.28	38.22	37.91	37.96	37.70	37.28	38.30
Al_2O_3	21.21	21.54	21.62	22.31	22.24	21.74	21.63	21.55	21.67	21.93
FeO	24.61	26.40	25.21	30.86	30.74	24.86	25.28	25.94	25.34	24.24
MnO	1.44	0.41	3.61	0.55	0.56	0.83	0.68	0.82	1.47	0.84
MgO	2.89	2.68	1.11	7.32	7.54	2.16	2.33	1.86	2.44	2.77
CaO	11.46	11.03	11.47	1.79	1.77	12.95	12.48	12.24	12.19	12.96
Sum	100.20	100.44	101.48	101.11	101.07	100.45	100.36	100.11	100.39	101.04
Si	3.026	3.009	3.012	2.962	2.958	2.977	2.983	2.981	2.943	2.977
Al	1.959	1.989	1.995	2.034	2.028	2.011	2.002	2.007	2.016	2.009
Fe	1.614	1.731	1.651	1.997	1.989	1.632	1.661	1.715	1.673	1.576
Mn	0.096	0.027	0.239	0.036	0.037	0.055	0.045	0.055	0.098	0.055
Mg	0.338	0.313	0.130	0.844	0.870	0.253	0.273	0.219	0.287	0.321
Ca	0.963	0.927	0.963	0.148	0.147	1.090	1.051	1.037	1.031	1.080
Almandine	53.6	57.7	55.4	66.0	65.4	53.9	54.8	56.7	54.1	52.0
Spessartine	3.2	0.9	8.0	1.2	1.2	1.8	1.5	1.8	3.2	1.8
Pyrope	11.2	10.4	4.3	27.9	28.6	8.3	9.0	7.2	9.3	10.6
Grossular	32.0	30.9	32.3	4.9	4.8	36.0	34.7	34.3	33.4	35.6
X_{Fe}	0.83	0.85	0.93	0.70	0.70	0.87	0.86	0.89	0.85	0.83

TiO_2, Cr_2O_3 <0.05.

TABLE 3 Composition of silicate minerals occurring together with garnet in KB860

	Phengite	Phengite	Paragonite	Paragonite	Chlorite	Chlorite	Epidote rim	Allanite core	Ree-zo	Amphibole barroisite	Amphibole barroisite	Plagioclase	Plagioclase
SiO_2	48.36	48.53	47.59	47.11	25.92	26.08	37.05	34.42	34.30	48.37	48.76	64.68	64.49
TiO_2	0.04	0.03	0.02	0.04						0.07	0.04		
Al_2O_3	33.51	32.96	39.73	39.41	22.85	22.44	30.43	27.26	26.24	11.29	11.96	22.69	22.34
FeO	1.85	1.94	0.17	0.27	23.49	23.89	4.92	4.92		13.38	13.17	0.1	0.08
MnO					0.3	0.27	0.11	0.01	0.03	0.17	0.12		
MgO	1.61	1.72	0.15	0.18	15.92	16.24	0.04	0.31	0.15	12.73	12.22		
CaO			0.17	0.22			23.60	21.49	21.54	9.05	8.71	3.59	3.63
Na_2O	0.74	0.69	7.59	7.31						2.16	2.57	9.6	9.34
K_2O	10.27	10.47	0.74	0.88						0.23	0.15	0.05	0.07
Total	96.47	96.38	96.17	95.43	88.48	88.92	96.15	88.41	82.26	97.45	97.7	100.71	99.95
Si	3.179	3.198	3.012	3.002	2.667	2.678	2.91	2.85	2.97	6.995	7.010	2.832	2.842
Al (IV)	0.821	0.802	0.988	0.998	1.333	1.322				1.005	0.990	1.171	1.160
Al (VI)	1.776	1.757	1.974	1.961	1.437	1.393	2.82	2.66	2.68	0.919	1.037		
Ti	0.002	0.001	0.001	0.002						0.008	0.004	0.004	0.003
Fe^{2+}	0.102	0.107	0.009	0.014	2.021	2.051	0.29	0.34		1.618	1.583		
Mn					0.026	0.023				0.021	0.015		
Mg	0.158	0.169	0.014	0.017	2.442	2.486			0.021	2.744	2.619	0.168	0.171
Ca			0.012	0.015			1.99	1.91	2.00	1.402	1.342	0.815	0.798
Na	0.094	0.088	0.931	0.904						0.606	0.716	0.003	0.004
K	0.861	0.880	0.060	0.070				0.606	0.716	0.042	0.028		
X_{Fe}	0.392	0.387			0.45	0.45				0.37	0.38		
An												17.1	17.6
Ab												82.6	82.0
Ab												0.3	0.4

Phengite: traces of Cr_2O_3, MnO, and CaO (<0.1 wt% each), mineral formulas normalized to 11 oxygen. Paragonite: traces of Cr_2O_3, MnO, mineral formulas normalized to 11 oxygen. Chlorite: traces of Ti, Cr, Ca, Na, and K (all <0.1 wt%), concentrations in wt%, formulas per 14 oxygen. Epidote: epidote rim = euhedral overgrowth on corroded REE-rich allanite (core). REE-zoisite = Fe-free zoisite containing about 15 wt%. REE_2O_3 total. Formulas normalized to 12.5 oxygen. Amphibole: formula based on 23 oxygen.
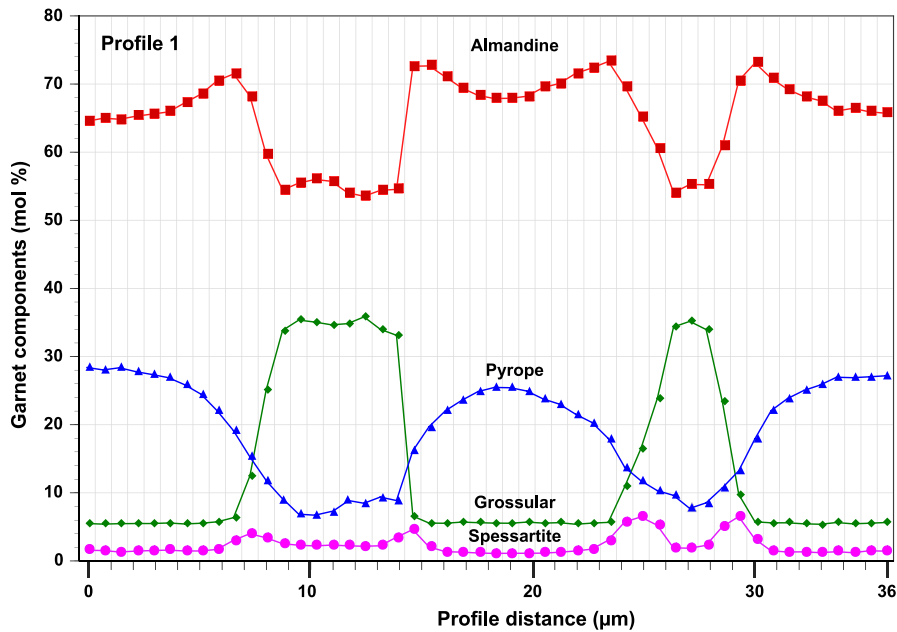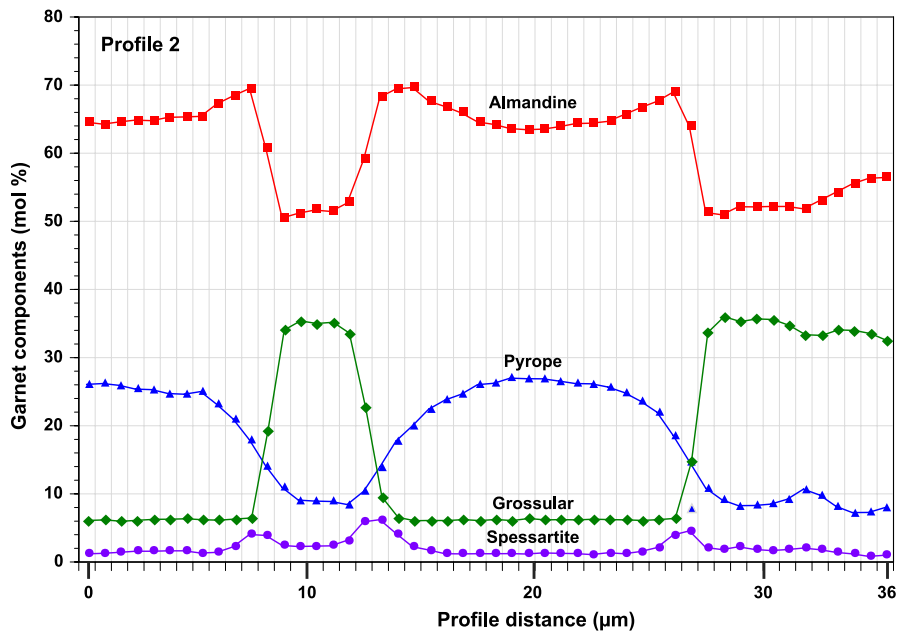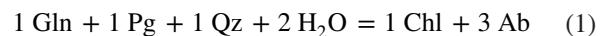
FIGURE 7 Garnet composition along profile 1 in KB860. It shows pyrope- and almandine-rich G-Grt, the fragments in Figure 3–5), separated by grossular-rich E-Grt. The Grs component changes abruptly at the contact of G-Grt and E-Grt, particularly well visible at distance 16 μm. Prp component changes smoothly at the contact over a distance of ~7 μm. Alm increases towards the rims of the G-Grt fragments and is lower in its interior (see also Figure 5). At the contact to E-Grt Alm drops off sharply (see at 16 μm). Sps enrichment is located at the contact of the two garnet

FIGURE 8 Garnet composition along profile 2 in KB860. It shows pyrope- and almandine-rich G-Grt, the fragments in Figure 3–5, separated by grossular-rich E-Grt. The Grs component changes immediately at the contact of G-Grt and E-Grt, particularly well visible at distance 16 μm. Prp component changes smoothly at the contact over a distance of ~7 μm. Alm increases towards the rims of the G-Grt fragments and is lower in its interior (see also Figure 5). At the contact to E-Grt Alm drops off abruptly (see at 8 μm). The enrichment in Sps is located exactly at the contact of the two garnet

chlorite-rich micaschist, excess H_2O conditions were generated by dehydration reactions progressing in the micaschists during E-Grt growth.

The observed E-Grt composition fits with the modelled garnet at ~530°C and 1.7 GPa. The composition of predicted garnet is 55 Alm–8 Prp–37 Grs compared with the analysed E-Grt 54 Alm–8 Prp–36 Grs (Table 2a and b). Computed and measured maximum Si phengite yield identical Si = 3.35 per formula unit normalized to 12 oxygen. The predicted assemblage at these $P–T$ conditions is (vol.%): Grt 10, Ph 37, Pg 23, Omp 9, Qz 16, Lws 5. The modelled assemblage differs from the observed assemblage in that the model predicts the presence of omphacite and lawsonite, neither of which are present in the rock. It is possible that Omp+Lws were originally present during E-Grt growth along a prograde subduction path, but were later removed from the matrix during complete greenschist facies recrystallization of the rock matrix. The model also fails to predict the presence of glaucophane at the E-Grt stage or pre-E-Grt stage for which there is textural evidence in the form of Ab-Chl pseudomorphs that may have formed by Reaction 1 (written with end-member phase components):

$$1\,Gln + 1\,Pg + 1\,Qz + 2\,H_2O = 1\,Chl + 3\,Ab \quad (1)$$

Reaction 1 requires external H_2O and typically occurs during retrogression of the rock. Some glaucophane may have been removed from the rock matrix by Reaction 2 (written with end-member phase components):
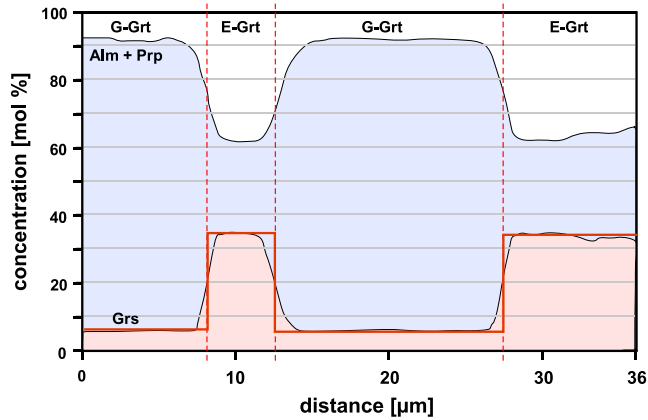
FIGURE 9 Garnet composition along profile 2 in KB860. It shows the grossular component and the total of pyrope and almandine component. In this representation, G-Grt and E-Grt have a constant composition. The somewhat smoothed transition at the contacts of the two garnet is mostly an effect of the limited resolution of the EMPA (~2–3 μm). The profile is close to a box shape. Vertical dashed lines mark the fracture contact of G-Grt and E-Grt

$$52\,Lws + 5\,Gln \rightarrow 26\,Clz/Ep + 3\,Chl + 10\,Pg + 27\,Qz + 74\,H_2O \quad (2)$$
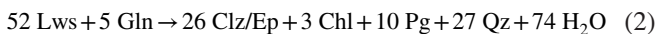
Reaction 2 links the assemblage present in the matrix of the rock to the pseudomorphed Gln and the predicted model Lws. This dehydration reaction progresses during decompression and replaces Lws with Clz-Pg pseudomorphs commonly found in retrogressed eclogites but rarely in eclogite facies micaschists. Chlorite is not predicted at the E-Grt P–T conditions.

4.4.3 | P–T conditions during recrystallization of the rock matrix

The rock matrix contains the assemblage Ph, Pg, Pl, Qz, Chl, Ep, and rare barroisitic amphibole. The composition of the matrix has been obtained by subtracting 10 vol.% of E-Grt from the E-Grt rock. This procedure is justified by the absence of dissolution and resorption textures, suggesting that E-Grt did not return material to the matrix during later stages of recrystallization (Figures 3 and 4). Furthermore, the matrix lacks the predicted omphacite and lawsonite for the E-Grt stage. This suggests that the matrix completely recrystallized under conditions different from those of the E-Grt stage.

Theriak phase equilibrium models suggest that the matrix assemblage equilibrated at ~470°C and 750 MPa. The predicted assemblage at this pressure and temperature is (mode in vol.% in brackets) Ph (43), Pg (3), Ep (10), Amp (3), Qz (16), Pl (19), and Chl (6), and matches the observed matrix assemblage. The modelled composition of the minerals— Phengite Si = 3.2, amphibole Gln = 35, epidote Clz = 85, chlorite X_{Fe} = 0.45, and plagioclase An = 17—matches the

measured composition of matrix minerals in sample KB860 excellently (Ph Si = 3.2, Brs Gln+Fe-Gln = 40, Ep Clz = 71, Chl X_{Fe} = 0.45, Pl An = 17; Table 3). However, the existence of two generations of K-white mica in some samples (main group Si = 3.2, late group Si = 3.0) in addition to rare early HP phengite (Si = 3.4) suggests that matrix recrystallization occurred in two steps. This is further supported by the presence of pure albite and texturally late chlorite in some samples. The latest assemblage in the matrix, Ab, Ms, Chl, Ep, Qz, is consistent with, for example, 350°C and 300 MPa.

5 | DISCUSSION

5.1 | A brief geotectonic interpretation of all derived P–T conditions

The P–T conditions at garnet growth and matrix recrystallization are summarized in Figure 11. Permian granulite facies metapelites (Kunz et al., 2018) with the assemblage Grt+Pl+Kfs+Qz+Bt+Sil, locally also Crd (Bucher et al., 2004; Diehl, Masson, & Stutz, 1952; Zucali et al., 2011), have been reported from the Valpelline Series of the Dent Blanche nappe overriding the TGU and ZSU (Figure 1). Manzotti and Zucali (2013) reported peak metamorphic conditions of 814 ± 40°C and 600–800 MPa for the Valpelline granulites similar to the P–T growth conditions of G-Grt reported here. Thus, the TGU slab may represent material from the Dent Blanche nappe tectonically emplaced in the ZSU.

Late garnet growth, which occurred at ~530°C and 1.7 GPa, represents eclogite facies conditions related to Alpine subduction. However, the conditions of E-Grt growth do not represent the peak conditions during Alpine subduction and associated high-P metamorphism at the maximum depth reached by the TGU unit. The latter has been derived from eclogites associated with the Grt-Ph schists and the reported peak P–T conditions are 580°C and 2.2 GPa (Weber & Bucher, 2015). The meta-ophiolites of the Zermatt–Saas nappe surrounding the TGU unit reached a maximum P–T ~600°C and 2.5 GPa depending on the location within the unit (Angiboust et al., 2009; Bucher et al., 2005; Bucher & Grapes, 2009; Weber & Bucher, 2015).

The two P–T points for the TGU rocks match the Alpine subduction–exhumation path for the Zermatt–Saas area (Figure 11). The TGU unit may have detached from the subducting slab at a shallower depth than most slices of the Zermatt–Saas meta-ophiolites. However, both the prograde and the retrograde return path are constrained to the serpentinite field of Figure 11 (see also fig. 15 in Weber & Bucher, 2015). Serpentinite within the Zermatt–Saas meta-ophiolite nappe do not show any evidence of antigorite replacement by olivine+talc or olivine+enstatite (Li, Rahn, & Bucher, 2004). This defines the upper limit of the serpentinite field on Figure 11. The lower limit is given by the replacement
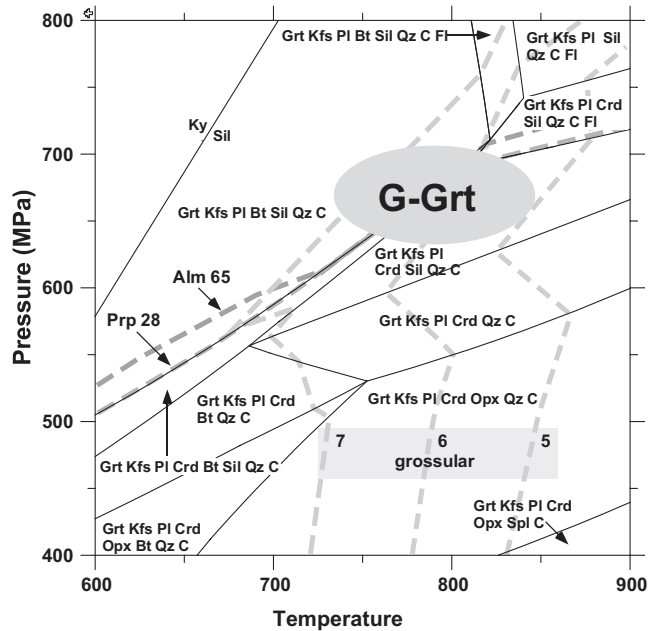
FIGURE 10 Assemblage stability diagram for the bulk rock composition of KB860 (Table 1). Oxidation state is defined by the presence of graphite. For software and conditions see text. The model assesses the growth conditions of G-Grt

FIGURE 11 Summary of metamorphic conditions: pre-Alpine granulite facies metamorphism forming G-Grt. Alpine high-P, low-T (HPLT) metamorphism produced E-Grt after fragmentation of G-Grt. Black star: peak P–T conditions reached by the TGU derived from TGU eclogites (Weber & Bucher, 2015). Black diamond: peak P–T conditions reached by the ZSU in the Zermatt area (average from Angiboust et al., 2009; Bucher et al., 2005; Bucher & Grapes, 2009). The HPLT path from low grade through E-Grt and the peak conditions for the TGU and ZSU marks a possible prograde path for Alpine subduction metamorphism. The exhumation path is constrained by the presence of stable Ol+Atg in the ZSU serpentinites and the derived conditions for the matrix recrystallization of the TGU Grt-Ph schists reported here

of olivine by brucite and antigorite. Metamorphic olivine is present as pure forsterite in all serpentinites and brucite replacing forsterite has not been reported from the Zermatt–Saas serpentinites (Li et al., 2004).

The derived P–T conditions (470°C, 750 MPa) for the matrix recrystallization can be placed on the derived exhumation path for subducted units in the Zermatt area (Weber & Bucher, 2015). Also, the latest recrystallization of the matrix at 350°C and 300 MPa matches that determined for the exhumation path (Figure 11). Matrix recrystallization may alternatively be related to deformation overprinting during Alpine nappe stacking. The derived P–T conditions of the matrix recrystallization correspond to the conditions for late Alpine greenschist facies overprint recorded by the rocks of the ophiolite nappe Zermatt–Saas (Barnicoat, Rex, Guise, & Cliff, 1995; Bearth, 1967; Bucher et al., 2005; Bucher & Grapes, 2009).

5.2 | Garnet porphyroblast formation

It follows from the models presented above that after granulite facies metamorphism the metapelitic gneiss contained ~26 vol.% G-Grt. Because of the high P–T conditions and the low Ca content (5 mol.% Grs) of G-Grt, it is assumed that it was chemically homogeneous and unzoned after granulite facies metamorphism. Consequently, all documented chemical zonation present in G-Grt developed after the fragmentation of the G-Grt porphyroblasts (Figures 3 and 4). The G-Grt fragments are concentrically chemically
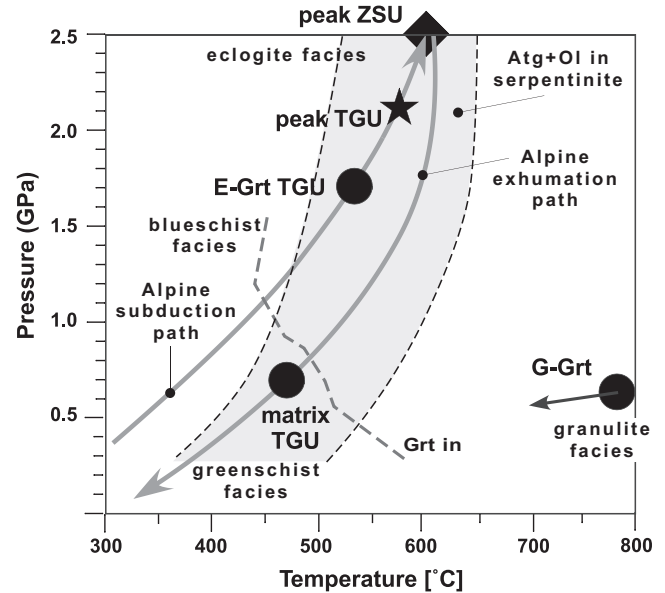
zoned; the pre-fragmentation porphyroblasts were unzoned. The G-Grt fragments have not been rotated or deformed later (e.g. flattened). Because the fragmentation fractures are sealed by E-Grt, fragmentation occurred during subduction prior to or concurrent with E-Grt formation. The space between the G-Grt fragments is almost exclusively occupied by E-Grt (Figures 4 and 5) with very few Qz and very rare Cal inclusions.

Late garnet between G-Grt fragments represents a mononmineralic seal of extension veins and may have formed as a precipitate from a fluid phase. The presence of small euhedral E-Grt grains in the matrix of the rocks suggests that this fluid was internally derived and not an external fluid precipitating E-Grt in the fractures. At this stage, the fluid was internally produced and buffered by the assemblage because E-Grt formed during prograde metamorphism of chlorite-rich micaschist. The textures (Figures 3 and 4) further suggest that the G-Grt porphyroblasts underwent brittle deformation at the early stages of subduction when E-Grt was formed (Figure 11). Brittle deformation also characterizes the early stages of subduction-related deformation of the nearby Allalin gabbro (Bucher & Grapes, 2009) in the Zermatt–Saas meta-ophiolite
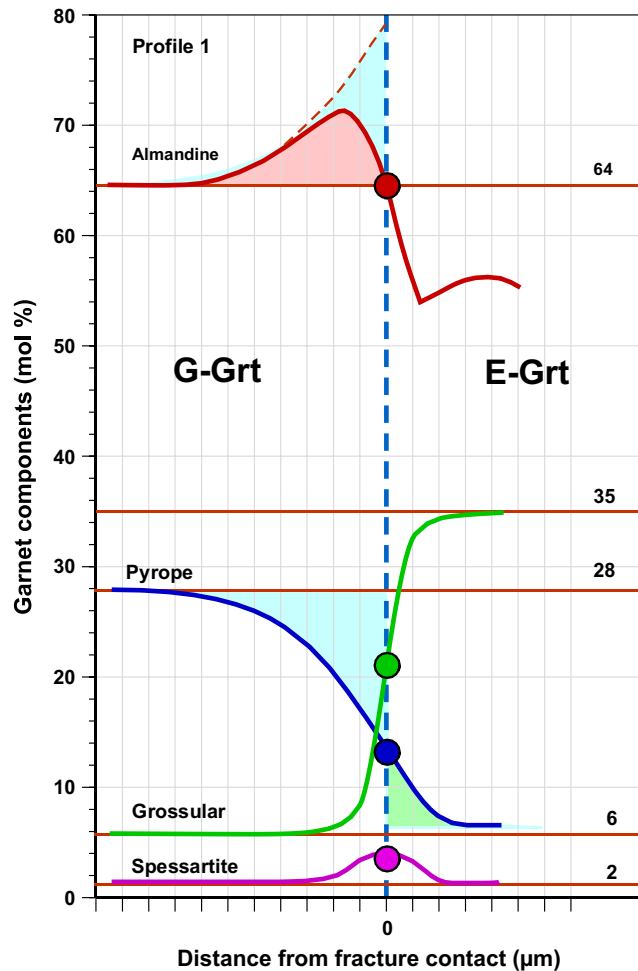
FIGURE 12 Intracrystalline diffusion in garnet. Data from profile 1 (see the supporting information, garnet profile 1). The original fracture contact between G-Grt and E-Grt is shown as a vertical dashed blue reference line (between position of analyses 11 and 12 on Table S1). It coincides with maximum Sps and with the discontinuity of the Grs concentration profile (see also Figure 9). The decrease in Prp in G-Grt towards the contact is compensated by an increase in Alm. The apparent decrease at the immediate contact of the two garnet is partly an effect of the EPMA resolution. The blue field limited by a dashed red curve along the Alm profile corresponds to the measured loss of Prp. The Alm in E-Grt is somewhat irregular but shows the lowest Alm concentrations along the profile. The Prp zone affected by intracrystalline diffusion reaches ~8 μm from the contact into G-Grt

(Figure 1). Fragmentation of granulite facies garnet in Bergen Arcs granulites (SW Norway) has been linked to subduction-related earthquakes by Austrheim et al. (2017).

At the time of fragmentation of the G-Grt porphyroblasts the rock matrix may still have had its granulite facies assemblage. Infiltration by dehydration water from deeper in the subduction zone converted and hydrated the high-grade assemblage into a chlorite-rich micaschist during the early stages of Alpine subduction-related metamorphism. There is no evidence that massive metasomatism was associated with
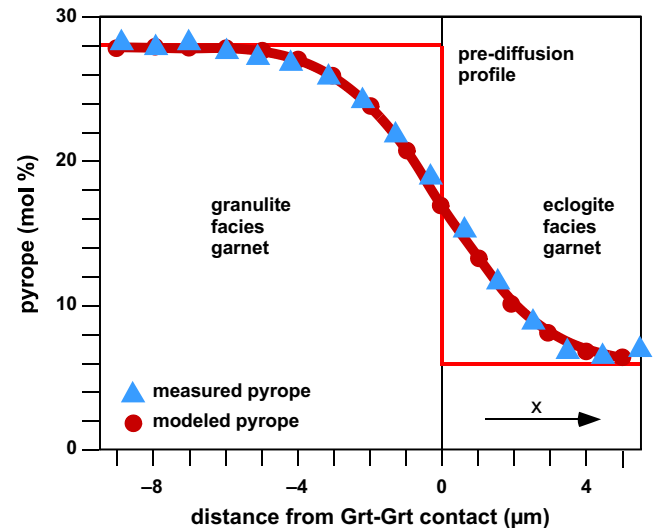

FIGURE 13 Model diffusion profile for Mg (red curve and red dots). The spreading of Mg from G-Grt to E-Grt stalled after *c.* 10 Ma using a diffusivity log $D_{Mg} = -25.8$ m^2/s. The temperature was ~530–550°C during much of the 10 Ma (maximum temperature 580°C). Measured Grt composition in mol.% Prp is shown as blue triangles (data taken from profile 2, Figure 8.)

hydration such as zoned contacts to the mafic rocks, monomineralic blackwalls, and similar features indicative of metasomatism. The suggested process is analogous to the reported subduction zone hydration of the Allalin gabbro (Bucher & Grapes, 2009) (Figure 1).

5.3 | Intracrystalline diffusion in G-Grt fragments and diffusion between G-Grt and E-Grt

The fractures that cut the original G-Grt are straight and cross each other at high angles (Figures 3 and 4) indicating that fracture sealing with E-Grt is caused by the formation of a new garnet generation rather than by replacement of the older garnet generation by resorption of garnet material. The textures indicate that after E-Grt precipitated in the veins, the garnet porphyroblasts (Figures 3 and 4) consisted of an inner region with homogeneous fragments of variable size of chemically unzoned G-Grt in a matrix of homogeneous unzoned E-Grt in the veins. The situation is depicted in Figure 9, showing the garnet composition profile 2 (Figure 8) with Alm and Prp combined referring to the pre-diffusion situation. Still, there is some 'diffusion-type' smooth boundary visible. This is related to the spatial resolution of the microprobe and the profile would approach a strict box shape with finer longitudinal resolution. The observed composition profiles (Figures 7 and 8) evolved from this idealized box-shaped composition profile (Figure 9). The detailed modifications of the originally sharp G- to E-Grt contact are depicted in Figure 12.

The smooth profiles for Mg (Figures 7, 8 and 12) result from diffusion between the two garnet at the scale of ~7–8 μm (14–16 μm total in both garnet). Diffusion smoothed out the originally sharp Mg profiles from 530°C, the temperature when the box-shaped starting configuration has been generated, to ~580°C, the derived maximum temperature reached by the TGU during the subduction process (Figure 12). The pressure difference between E-Grt generation and detachment of the TGU from the slab is ~0.4–0.5 GPa (Figure 11), corresponding to ~13 km depth difference, which can be travelled by the slab in *c.* 2 Ka (kilo year), assuming a plate velocity of 6 cm/year, corresponding to a vertical velocity of 4 cm/year. However, diffusion continued during exhumation until it became very slow at low temperature. Assuming that this 'blocking temperature' is close to 500°C, exhumation amounted to 50 km vertical difference from the return point. Typical orogenic exhumation velocities are 4 mm/year (Zhang et al., 2018), which results in *c.* 12.5 Ma for the retrograde section of the path from 580 to 500°C. The smooth Mg profiles thus represent the result of diffusion in the order of 13 Ma. Most of the smooth Mg profiles probably resulted from diffusion close to the maximum temperature of ~580°C.

This tectonically derived time-scale for the development of the stranded diffusion profile (Figures 7 and 8) from the original box-shaped profile (Figure 9) can be validated from computed diffusion profiles using diffusivity data. The concentration progression due to diffusion of Mg or pyrope in Grt along a profile can be computed from Equation 3, as given by Crank (1975):

$$C(x,t) = \frac{C_0}{2} \left[1 - \mathrm{erf}\left(\frac{x}{\sqrt{4Dt}} \right) \right] \qquad (3)$$

where $C(x,t)$ is the concentration of the diffusing component at distance x (m) and after time t (s), C_0 denotes the concentration of the diffusing component at distance $x = 0$ (m), and D (m²/s) represents the diffusion coefficient (mass diffusivity). Figure 13 shows the modelled diffusion profile of Mg spreading (expressed as pyrope component in Grt in mol.%) from G-Grt to E-Grt after 10 Ma and for log $D = -25.8$ m²/s (red dots and red curve). The measured profile from Figure 8 is shown with blue symbols. This diffusivity is somewhat below the diffusivities given by Carlson (2006) for four diffusing components in garnet (his fig. 8). The compiled data (Carlson, 2006) range from −23.5 to −25.0 at 580°C. Our derived log diffusivity of −25.8 m²/s may suggest that diffusion progressed at <580°C, probably in the range of 530–550°C. Alternatively, the diffusion may have progressed during a shorter period of time. Using the average log $D_{\mathrm{Mg}} = -24$ m²/s at 580°C (Carlson, 2006) the measured Mg distribution develops in less than *c.* 100 Ka, which we consider to be an unrealistically short time.

However, because Mg diffusion is coupled with Fe diffusion as a result of the charge balance requirement, consequently Mg cannot diffuse faster than Fe. Using the lower limit of log $D_{\mathrm{Fe}} = -25.3$ m²/s at 580°C (Carlson, 2006), the observed profile (Figure 13) develops in relatively short 2 Ma. Also, this result suggests that much of the observed diffusion profile developed at < 580°C.

Distinct thin Mn-rich rims around the fragments of G-Grt could be the result of some garnet resorption after fragmentation (de Béthune, Laduron, & Bocquet, 1975). The Mn profile is symmetrical with the maximum exactly at the contact of the two garnet (Figure 12). An alternative and more plausible interpretation for garnet of the TGU schists is that they formed by fractionating Mn from the fluid in the fracture into the very first E-Grt formed. The Mn profile has been flattened later by diffusion to some extent. Thus, the Mn rim is present on both sides of the contact. The feature measures less than 4 μm across (Figure 12). The proposed process would explain the constant thickness of the Mn rims and the absence of irregularly curved resorption textures. The very sharp boundary for Ca indicates that diffusion of Ca is inefficient at the scale of less than 2 μm at 580°C; log $D_{\mathrm{Ca}} = -27.5$ m²/s at the derived temperature of 530–550°C is consistent with 10 Ma for profile development.

This data interpretation is in agreement with garnet diffusion data and models showing that diffusion is at a length scale of a few micrometres at temperatures as low as 500°C (Caddick et al., 2010; Carlson, 2006). It is also evident that Ca diffusion is at a much lower length scale than Mg diffusion in accordance with experimental and empirical diffusivity data in garnet (Carlson, 2006; Chernoff & Carlson, 1997; Loomis, Ganguly, & Elphick, 1985).

An interesting feature of the garnet composition profiles is the marked increase of Alm in G-Grt towards the contact with E-Grt where Alm is much lower than in G-Grt. This feature is clearly visible on both profiles (Figures 7 and 8). It is caused by the diffusion of Mg from G-Grt to E-Grt. The vacant Mg positions in G-Grt must be replaced by Fe to maintain charge balance. This leads to diffusion of Fe from a region with low Fe concentration (E-Grt) towards the rim of G-Grt. This process is known as uphill diffusion (Borinski, Hoppe, Chakraborty, Ganguly, & Bhowmik, 2012; Ganguly, 2002; Lesher, 1994), particularly recognized in spinodal decomposition of mineral solid solutions. The compositional features of the TGU garnet along the two profiles are excellent examples of uphill diffusion.

The total amount of Mg transferred from G-Grt to E-Grt must be exactly matched by an equal amount of Fe transferred from E-Grt to G-Grt (Figure 12). This leads to a sharp discontinuity in the Fe profile that cannot be fully resolved because of the limited resolution of the EPMA. The blue area under the Prp curve in Figure 12 shows the loss of Mg by

G-Grt. It must be matched by the Mg gained by E-Grt (green area). However, the Mg loss by G-Grt is apparently not exactly equal to the Mg gain by E-Grt. This is probably related to the fact that the profile data are from a two-dimensional section and the full 3D geometry is not known. A strict loss–gain balance is expected along the 3D diffusion path. The Fe gained by uphill diffusion (red area of Figure 12) is seemingly smaller than the Mg loss (blue area). This mismatch is caused by the limited resolution of the microprobe and disappears if the apparent gain of Ca and Mn by G-Grt are added to the red Fe area.

6 | CONCLUSIONS

Large garnet porphyroblasts in garnet–phengite schist occurring in a slab of continental basement (TGU) in the ZSU show complex internal compositional patterns. An early garnet generation has a composition typical of granulite facies garnet (G-Grt). The large G-Grt porphyroblasts were later fractured and fragmented. The fractures and fragments of G-Grt have been overgrown by a late grossular-rich garnet generation typical of HPLT metamorphism (E-Grt).

The garnet of the GPS are polymetamorphic (or polycyclic in current geologic parlance) and the internal garnet textures are complex. The detailed compositional and textural features suggest that fragmentation occurred during subduction. Composition profiles indicate that the contacts between G-Grt fragments and sealing E-Grt have been modified by cation diffusion. The profiles (Figures 7, 8 and 12) suggest that Ca is not exchanged between G- and E-Grt garnet in contact at the scale of 1 μm, whereas Fe and Mg diffuse efficiently at 580°C at the scale of several micrometres at the time-scale of some Ma (*c*. 10 Ma). The efficient intracrystalline Mg diffusion forces uphill diffusion of Fe to maintain charge balance in G-Grt, losing Mg to E-Grt. The features of the TGU garnet porphyroblasts show that garnet growth histories may be dramatically more complex than those of often studied and theoretically modelled single-event prograde garnet.

ORCID

Kurt Bucher https://orcid.org/0000-0003-1399-3614

REFERENCES

Angiboust, S., Agard, P., Jolivet, L., & Beyssac, O. (2009). The Zermatt-Saas ophiolite: The largest (60-km wide) and deepest (c. 70–80 km) continuous slice of oceanic lithosphere detached from a subduction zone? *Terra Nova*, *21*, 171–180.

Austrheim, H., Dunkel, K. G., Plümper, O., Ildefonse, B., Liu, Y., & Jamtveit, B. (2017). Fragmentation of wall rock garnets during deep crustal earthquakes. *Science Advances*, *3*(2), 1–7. e1602067. https://doi.org/10.1126/sciadv.1602067

Barnicoat, A. C., Rex, D. C., Guise, P. G., & Cliff, R. A. (1995). The timing of and nature of green schist facies deformation and metamorphism in the upper Pennine Alps. *Tectonics*, *14*, 279–293. https://doi.org/10.1029/94TC02017

Baxter, E. F., Caddick, M. J., & Dragovic, B. (2017). Garnet: A rock-forming mineral petrochronometer. *Reviews in Mineralogy & Geochemistry*, *83*, 469–533. https://doi.org/10.2138/rmg.2017.83.15

Bearth, P. (1967). *Die ophiolithe der Zone von Zermatt-Saas Fee*. Beiträge zur geologischen Karte der Schweiz. N.F. 132, p. 130.

Berman, R. B. (1988). Internally consistent thermodynamic data for minerals in system: $Na_2O-K_2O-CaO-MgO-FeO-Fe_2O_3-Al_2O_3-SiO_2-TiO_2-H_2O-CO_2$. *Journal of Petrology*, *29*, 445–522.

Borinski, S. A., Hoppe, U., Chakraborty, S., Ganguly, J., & Bhowmik, S. K. (2012). Multicomponent diffusion in garnets I: General theoretical considerations and experimental data for Fe–Mg systems. *Contributions to Mineralogy and Petrology*, *16*, 571–586. https://doi.org/10.1007/s00410-012-0758-0

Bowtell, S. A., Cliff, R. A., & Barnicoat, A. C. (1994). Sm-Nd isotopic evidence on the age of eclogitization in the Zermatt-Sass ophiolite. *Journal of Metamorphic Geology*, *12*, 187–196.

Bucher, K., Dal Piaz, G. V., Oberhänsli, R., Gouffon, Y., Martinotti, G., & Polino, R. (2004). Blatt 1347 Matterhorn. Geol. Atlas Schweiz 1:25000, Erläuterungen 107, p. 73.

Bucher, K., Fazis, Y., de Capitani, C., & Grapes, R. (2005). Blueschists, eclogites and decompression assemblages of the Zermatt-Saas ophiolite: High-pressure metamorphism of subducted Tethys lithosphere. *American Mineralogist*, *90*, 821–835. https://doi.org/10.2138/am.2005.1718

Bucher, K., & Grapes, R. (2009). The eclogite-facies Allalin Gabbro of the Zermatt-Saas Ophiolite, Western Alps: A Record of subduction zone hydration. *Journal of Petrology*, *50*, 1405–1442. https://doi.org/10.1093/petrology/egp035

Caddick, M. J., Konopasek, J., & Thompson, A. B. (2010). Preservation of garnet growth zoning and the duration of prograde metamorphism. *Journal of Petrology*, *51*, 2327–2347. https://doi.org/10.1093/petrology/egq059

Carlson, W. D. (2006). Rates of Fe, Mg, Mn and Ca diffusion in garnet. *American Mineralogist*, *91*, 1–11. https://doi.org/10.2138/am.2006.2043

Carmichael, R. S. (1989). *Practical handbook of physical properties of rocks and minerals* (p. 834). Boca Raton, FL: CRC Press.

Chen, N.-S., Sun, M., You, Z.-D., & Malpas, J. (1998). Well-preserved garnet growth zoning in granulite from the Dabie Mountains, central China. *Journal of Metamorphic Geology*, *16*, 213–222. https://doi.org/10.1111/j.1525-1314.1998.00074.x

Chernoff, C. B., & Carlson, W. D. (1997). Disequilibrium for Ca during growth of pelitic garnet. *Journal of Metamorphic Geology*, *15*, 421–438. https://doi.org/10.1111/j.1525-1314.1997.00026.x

Crank, J. (1975). *The mathematics of diffusion*. Oxford, UK: Clarendon Press, 414 pp.

Cutts, K. A., Kinny, P. D., Strachan, R. A., Hand, M., Kelsey, D. E., Emery, M., … Leslie, A. G. (2010). Three metamorphic events recorded in a single garnet: Integrated phase modelling, in situ LA-ICPMS and SIMS geochronology from the Moine Supergroup, NW Scotland. *Journal of Metamorphic Geology*, *28*, 249–267.

de Béthune, P., Laduron, D., & Bocquet, J. (1975). Diffusion processes in resorbed garnets. *Contributions to Mineralogy and Petrologie*, *50*, 197–204. https://doi.org/10.1007/BF00371039

de Capitani, C., & Petrakakis, K. (2010). The computation of equilibrium assemblage diagrams with Theriak/Domino software. *American Mineralogist*, *95*, 1006–1016. https://doi.org/10.2138/am.2010.3354

Diehl, E. A., Masson, R., & Stutz, A. H. (1952). Contributo alla conoscenza del ricoprimento della Dent Blanche. *Memorie Degli Istituti Di Geologia E Mineralogia Dell'università Di Padova*, *17*, 1–52.

Droop, G. T. R., & Bucher-Nurminen, K. (1984). Reaction textures and metamorphic evolution of sapphirine-bearing granulites from the Gruf complex, Italian Central Alps. *Journal of Petrology*, *25*, 766–803. https://doi.org/10.1093/petrology/25.3.766

Feenstra, A., Petrakakis, K., & Rhede, D. (2007). Variscan relics in Alpine high-P pelitic rocks from Samos (Greece): Evidence from multistage garnet and its included minerals. *Journal of Metamorphic Geology*, *25*, 1011–1033. https://doi.org/10.1111/j.1525-1314.2007.00741.x

Florence, F. P., & Spear, F. S. (1991). Effects of diffusional modification of garnet growth zoning on P-T path calculations. *Contributions to Mineralogy and Petrology*, *107*, 487–500. https://doi.org/10.1007/BF00310683

Gaidies, F., Pattison, D. R. M., & de Capitani, C. (2011). Toward a quantitative model of metamorphic nucleation and growth. *Contributions to Mineralogy and Petrology*, *162*, 975–993. https://doi.org/10.1007/s00410-011-0635-2

Gaidies, F., Petley-Ragan, A., Charkraboty, S., Dasgupta, S., & Jones, P. (2015). Constraining the conditions of Barrovian metamorphism in Sikkim, India: P-T–t paths of garnet crystallization in the Lesser Himalayan Belt. *Journal of Metamorphic Geology*, *33*, 23–44.

Ganguly, J. (2002). Diffusion kinetics in minerals: Principles and applications to tectono-metamorphic processes. *EMU Notes in Mineralogy*, *4*, 271–309.

George, F. R., & Gaidies, F. (2017). Characterisation of a garnet population from the Sikkim Himalaya: Insights into the rates and mechanisms of porphyroblast crystallisation. *Contribution to Mineralogy and Peterology*, *172*, 57.

Groppo, C., Beltrando, M., & Compagnoni, R. (2009). The P-T path of the ultra-high pressure Lago di Cignana and adjoining high-pressure meta-ophiolitic units: Insights into the evolution of the subducting Tethyan slab. *Journal of Metamorphic Geology*, *27*, 207–231.

Hawthorne, F. C., Oberti, R., Harlow, G. E., Maresch, W. V., Martin, R. F., Schumacher, J. C., & Welch, M. D. (2012). Nomenclature of the amphibole supergroup. *American Mineralogist*, *97*, 2031–2048. https://doi.org/10.2138/am.2012.4276

Herron, M. M. (1988). Geochemical classification of terrigenous sands and shales from core or log data. *Journal of Sedimentary Research*, *58*, 820–829.

Hollister, L. S. (1966). Garnet zoning: An interpretation based on the Rayleigh fractionation model. *Science*, *154*, 1647–1651. https://doi.org/10.1126/science.154.3757.1647

Jedlicka, R., Faryad, S. W., & Hauzenberger-Jedlicka, C. (2015). Prograde Metamorphic History of UHP Granulites from the Moldanubian Zone (Bohemian Massif). Revealed by Major Element and Y + REE Zoning in Garnets. *Journal of Petrology*, *56*, 2069–2088.

Keller, J. M., de Capitani, C., & Abart, R. (2005). A quaternary solution model for white micas based on natural coexisting phengite–paragonite pairs. *Journal of Petrology*, *46*, 2129–2144. https://doi.org/10.1093/petrology/egi050

Kelly, E. D., Hoisch, T. D., Wells, M. L., Vervoort, J. D., & Beyene, M. A. (2015). An Early Cretaceous garnet pressure–temperature path recording synconvergent burial and exhumation from the hinterland of the Sevier orogenic belt, Albion Mountains, Idaho. *Contributions to Mineralogy and Peterology*, *170*, 2–22. https://doi.org/10.1007/s00410-015-1171-2

Klemm, O. (2005). Die metamorphe Entwicklung der metabasischen und metasedimentären Anteile der Zermatter Ophiolithe im Bereich Lichenbretter – Oberer Theodulgletscher, Wallis, Schweiz. *Unpublished MSc thesis* (Diplomarbeit), University of Freiburg, Germany, p. 115.

Konrad-Schmolke, M., Zack, T., O'Brien, P. J., & Jacob, D. E. (2008). Combined thermodynamic and rare earth element modeling of garnet growth during subduction: Examples from ultrahigh-pressure eclogite of the Western Gneiss Region, Norway. *Earth and Planetary Science Letters*, *272*, 488–498.

Kunz, B. E., Manzotti, P., von Niederhäusern, B., Engi, M., Darling, J. R., Giuntoli, F., & Lanari, P. (2018). Permian high-temperature metamorphism in the Western Alps (NW Italy). *International Journal of Earth Sciences*, *107*, 203–229. https://doi.org/10.1007/s00531-017-1485-6

Lapen, T. J., Johnson, C. M., Baumgartner, L. P., Mahlen, N. J., Beard, B. L., & Amato, J. M. (2003). Burial rates during prograde metamorphism of an ultra-high-pressure terrane: An example from Lago di Cignana, western Alps, Italy. *Earth and Planetary Science Letters*, *215*, 57–72. https://doi.org/10.1016/S0012-821X(03)00455-2

Lesher, C. E. (1994). Kinetics of Sr and Nd exchange in silicate liquids: Theory, experiments, and applications to uphill diffusion, isotopic equilibration, and irreversible mixing of magmas. *Journal of Geophysical Research*, *99*, 9585–9604. https://doi.org/10.1029/94JB00469

Li, X.-P., Rahn, M., & Bucher, K. (2004). Serpentinites of the Zermatt-Saas ophiolite complex and their texture evolution. *Journal of Metamorphic Geology*, *22*, 159–178.

Loomis, T. P. (1983). Compositional zoning of crystals: A record of growth and reaction history. In S. K. Saxena & S. K. Saxena (Eds.), *Kinetics and equilibrium in mineral reactions* (pp. 1–60). New York, NY: Springer.

Loomis, T. P., Ganguly, J., & Elphick, S. C. (1985). Experimental determination of cation diffusivities in aluminosilicate garnets II. Multicomponent simulation and tracer diffusion coefficients. *Contributions to Mineralogy and Petrology*, *90*, 45–51. https://doi.org/10.1007/BF00373040

Lu, Z., Zhang, L., Du, J., & Bucher, K. (2009). Petrology of coesite-bearing eclogite from Habutengsu Valley, western Tianshan, NW China and its tectonometamorphic implication. *Journal of Metamorphic Geology*, *27*, 773–787. https://doi.org/10.1111/j.1525-1314.2009.00845.x

Manzotti, P., & Ballèvre, M. (2013). Multistage garnet in high-pressure metasediments: Alpine overgrowths on Variscan detrital grains. *Geology*, *41*, 1151–1154. https://doi.org/10.1130/G34741.1

Manzotti, P., & Zucali, M. (2013). The pre-Alpine tectonic history of the Austroalpine continental basement in the Valpelline unit (Western

Italian Alps). *Geological Magazine*, *150*, 153–172. https://doi.org/10.1017/S0016756812000441

Markl, G., Bäuerle, J., & Grujic, D. (2000). Metamorphic evolution of Pan-African granulite facies metapelites from Southern Madagascar. *Precambrian Research*, *102*, 47–68. https://doi.org/10.1016/S0301-9268(99)00099-6

Masberg, P. (2000). Garnet growth in medium-pressure granulite facies metapelites from the central Damara Orogen: Igneous versus metamorphic history. *Communications of the Geological Survey of Namibia*, *12*, 131–141.

Rebay, G., Spalla, M. I., & Zanoni, D. (2012). Interaction of deformation and metamorphism during subduction and exhumation of hydrated oceanic mantle: Insights from the Western Alps. *Journal of Metamorphic Geology*, *30*, 687–702. https://doi.org/10.1111/j.1525-1314.2012.00990.x

Reinecke, T. (1991). Very-high-pressure metamorphism and uplift of coesite-bearing metasediments from the Zermatt-Saas zone, Western Alps. *European Journal of Mineralogy*, *3*, 7–17. https://doi.org/10.1127/ejm/3/1/0007

Reinecke, T. (1998). Prograde high to ultrahigh pressure metamorphism and exhumation of oceanic sediments at Lago di Cignana, Zermatt Saas Zone, western Alps. *Lithos*, *42*, 147–190.

Rubatto, D., Gebauer, D., & Fanning, M. (1998). Jurassic formation and Eocene subduction of the Zermatt-Saas-Fee ophiolites: Implications for the geodynamic evolution of the Central and Western Alps. *Contributions to Mineralogy and Petrology*, *132*, 269–287. https://doi.org/10.1007/s004100050421

Rubatto, D., & Hermann, J. (2003). Zircon formation during fluid circulation in eclogites (Monviso, Western Alps): Implications for Zr and Hf budget in subduction zones. *Geochimica et Cosmochimica Acta*, *67*, 2173–2187. https://doi.org/10.1016/S0016-7037(02)01321-2

Thigpen, J. R., Law, R. D., Loehn, C. L., Strachan, R. A., Tracy, R. J., Lloyd, G. E., … Brown, S. J. (2013). Thermal structure and tectonic evolution of the Scandian orogenic wedge, Scottish Caledonides: Integrating geothermometry, deformation temperatures and conceptual kinematic-thermal models. *Journal of Metamorphic Geology*, *31*, 813–842. https://doi.org/10.1111/jmg.12046

Weber, S., & Bucher, K. (2015). An eclogite-bearing continental tectonic slice in the Zermatt-Saas high-pressure ophiolites at Trockener Steg (Zermatt, Swiss Western Alps). *Lithos*, *232*, 336–359. https://doi.org/10.1016/j.lithos.2015.07.010

Weber, S., Sandmann, S., Miladinova, I., Fonseca, R. O. C., Froitzheim, N., Münker, C., & Bucher, K. (2015). Dating the Initiation of Piemonte-Liguria Ocean Subduction: Lu–Hf Garnet Chronometry of Eclogites From the Theodul Glacier Unit (Zermatt–Saas Zone, Switzerland). *Swiss Journal of Geosciences*, *108*, 183–199. https://doi.org/10.1007/s00015-015-0180-5

Whitney, D. L., & Evans, B. W. (2010). Abbreviations for names of rock-forming minerals. *American Mineralogist*, *95*, 185–187. https://doi.org/10.2138/am.2010.3371

Woodworth, G. (1977). Homogenization of zoned garnets from pelitic schists. *Canadian Mineralogist*, *15*, 230–242.

Yardley, B. W. D. (1977). An empirical study of diffusion in garnet. *American Mineralogist*, *62*, 793–800.

Zhang, L., Chu, X., Zhang, L., Fu, B., Bader, T., Du, J., & Li, X. (2018). The early exhumation history of the Western Tianshan UHP metamorphic belt, China: New constraints from titanite U-Pb geochronology and thermobarometry. *Journal of Metamorphic Geology*, *36*(5), 631–651. https://doi.org/10.1111/jmg.12422

Zucali, M., Manzotti, P., Diella, V., Pesenti, C., Rispendente, A., Darling, J., & Engi, M. (2011). Permian tectonometamorphic evolution of the Dent-Blanche Unit (Austroalpine domain, Western Italian Alps). *Rendiconti Online della Società Geologica Italiana*, *15*, 133–136.

SUPPORTING INFORMATION

Additional supporting information may be found online in the Supporting Information section at the end of the article.

Table S1. Composition profile 1 across porphyroblastic garnet from KB860.

Table S2. Composition profile 2 across porphyroblastic garnet from KB860.